International Journal of Nanomedicine

Dovepress
open access to scientific and medical research

Open Access Full Text Article

ORIGINAL RESEARCH

Folic acid-modified ginsenoside Rg5-loaded bovine serum albumin nanoparticles for targeted cancer therapy in vitro and in vivo

This article was published in the following Dove Press journal:
International Journal of Nanomedicine

Yanan Dong[1–3]
Rongzhan Fu[1–3]
Jing Yang[1–3]
Pei Ma[1–3]
Lihua Liang[2]
Yu Mi[1–3]
Daidi Fan[1–3]

[1]Shaanxi Key Laboratory of Degradable Biomedical Materials, School of Chemical Engineering, Northwest University, Xi'an, Shaanxi 710069, People's Republic of China; [2]Shaanxi R&D Center of Biomaterials and Fermentation Engineering, School of Chemical Engineering, Northwest University, Xi'an, Shaanxi 710069, People's Republic of China; [3]Biotech & Biomed Research Institute, Northwest University, Xi'an, Shaanxi 710069, People's Republic of China

Background and purpose: Ginsenoside Rg5 (Rg5), a triterpene saponin, extracted from the natural herbal plant ginseng, is one of the most potent anticancer drugs against various carcinoma cells. However, the therapeutic potential of Rg5 is limited by its low solubility in water, poor bioavailability, and nontargeted delivery. Therefore, we prepared folic acid (FA)-modified bovine serum albumin (BSA) nanoparticles (FA-Rg5-BSA NPs) to improve the therapeutic efficacy and tumor targetability of Rg5.

Methods: Various aspects of the FA-Rg5-BSA NPs were characterized, including size, polydispersity, zeta potential, morphology, entrapment efficiency (EE), drug loading (DL), in vitro drug release, thermal stability, in vitro cytotoxicity, cell apoptosis, cellular uptake, in vivo antitumor effects and in vivo biodistribution imaging.

Results: The FA-Rg5-BSA NPs showed a particle size of 201.4 nm with a polydispersity index of 0.081, uniform spherical shape, and drug loading of 12.64±4.02%. The aqueous solution of FA-Rg5-BSA NPs had favorable stability for 8 weeks at 4°C. The FA-Rg5-BSA NPs dissolved under acidic conditions. Moreover, the Rg5-BSA NPs and FA-Rg5-BSA NPs had advanced anticancer activity compared with Rg5 in MCF-7 cells, while poor cytotoxicity was observed in L929 cells. The FA-Rg5-BSA NPs facilitated cellular uptake and induced apoptosis in MCF-7 cells. In addition, in an MCF-7 xenograft mouse model, the in vivo antitumor evaluation revealed that FA-Rg5-BSA NPs were more effective in inhibiting tumor growth than Rg5 and Rg5-BSA NPs. The in vivo real-time bioimaging study showed that the FA-Rg5-BSA NPs exhibited superior tumor accumulation ability.

Conclusion: The results suggested that FA-Rg5-BSA NPs could serve as a promising system to improve the antitumor effect of Rg5.

Keywords: ginsenoside Rg5, drug delivery, nanoparticles, antitumor activity, human MCF-7 breast cancer cells

Introduction

In modern society, cancer is a serious threat to public health worldwide and imposes a heavy economic and psychological burden on the country, society and individuals. According to the current medical technology, the typical scientific treatments for cancer are surgery, radiation therapy and chemotherapy.[1,2] Chemotherapy is now a commonly and widely used strategy in treating solid tumors. Unfortunately, conventional chemotherapy usually leads to numerous unfavorable effects such as poor selectivity toward cancer cells, low drug concentration accumulation at the tumor-targeting site, and multidrug resistance in the body.[3] Commercial formulations,

Correspondence: Yu Mi; Daidi Fan
Shaanxi Key Laboratory of Degradable Biomedical Materials, School of Chemical Engineering, Northwest University, 229 North Taibai Road, Xi'an, Shaanxi 710069, People's Republic of China
Email mi_yu@nwu.edu.cn; fandaidi@nwu.edu.cn

submit your manuscript | www.dovepress.com
DovePress
http://doi.org/10.2147/IJN.S210882

such as Taxol®, can cause allergic reactions and severe toxicity to patients.[4] These shortcomings result in low therapeutic effects. Simultaneously, various highly active pharmacological anticancer drugs are being developed. One of them is ginsenoside Rg5 (Rg5), extracted from ginseng, which is a well-known herbal plant in Eastern countries.[5] Ginsenosides, the main active ingredients of ginseng, are triterpene saponins. They possess extensive pharmacological activities, including anti-tumor, anti-inflammatory, anti-angiogenic, anti-allergenic, anti-oxidant, anti-aging, and anti-diabetic activities.[6,7] Rg5, a main rare ginsenoside, has the unique biological properties.[8] Recently, researchers have paid close attention to Rg5 for its anticancer potency in several kinds of carcinoma, including esophageal, gastric, breast, and cervical cancer.[9–11] However, the low water solubility, poor bioavailability, and short biological half-time of Rg5 limit its medical application.[12,13] Although polyethylene glycol (PEG) 400, polyethoxylated castor oil, ethanol or Tween 80 could enhance the solubility of Rg5, a high concentration of the solvent may cause serious side effects. Therefore, we urgently need to find new avenues for improving the current cancer treatment regimens to overcome this medical problem.

In recent years, researchers have been focused on the combination of nanomedicine and oncology in the context of nanotechnology. The abovementioned deficiencies of Rg5 could perhaps be overcome by targetable, biodegradable and biocompatible nanoscale drug delivery systems, such as liposomes, micelles, dendrimers, and nanoparticles (NPs).[14] Albumin as vehicles have been extensively investigated for drug delivery applications, to enhance the solubility and therapeutic effect of drugs.[15] The drugs can bind to albumin with a certain affinity and then release into the cells under weakly acidic conditions. Albumin-based NPs deliver drugs to cancer cells while decreasing toxicity in healthy cells by two approaches: passive and active targeting.[16] In the passive targeting approach, bovine serum albumin (BSA)-based nanocarriers enable drug delivery due to the intrinsic natural properties of BSA.[17–19] These nanocarriers are transported by albumin receptor gp60-mediated transcytosis or the enhanced permeability and retention (EPR) effect in the hostile tumor microenvironment.[18,20,21] In the active targeting approach, BSA has certain functional groups to be covalently modified by target molecules. One of these molecules, folic acid (FA) is famous for its unique advantages, including stability, low immunogenicity, and high binding affinity with the FRα receptors that are overexpressed in several cancer cells, not the normal cells.[22–24] FA-modified BSA nanoparticles recognize the FRα receptors on the cells and subsequently enter the specific cells via receptor-mediated endocytosis, achieving drug accumulation in tumors, targeted delivery in cancer cells and side effect reduction in healthy tissues.[25]

In the present work, we prepared Rg5-loaded BSA nanoparticles using the desolvation method and then modified them with FA via an amidation reaction. The resulting FA-Rg5-BSA NPs were characterized by Fourier transform infrared (FT-IR) spectroscopy and nuclear magnetic resonance (^{1}H NMR) for material structures, scanning electron microscopy (SEM) and transmission electron microscopy (TEM) for surface morphology, dynamic light scattering (DLS) for particle size and zeta potential, and high-performance liquid chromatography (HPLC) for drug loading and release. Then, in vitro biological studies of FA-Rg5-BSA NPs were performed using a series of assays associated with cell viability, apoptosis, and cellular uptake. Finally, the in vivo antitumor effect and the real-time bioimaging evaluation for FA-Rg5-BSA NPs were assessed.

Materials and methods

Chemicals and reagents

Ginsenoside Rg5 (purity>95%) was purchased from Chengdu Puruifa Technology Co., Ltd. (Sichuan, China). Bovine serum albumin (BSA, fraction V, purity>96%) was obtained from Amresco (Solon, OH, USA). Folic acid (FA, purity≥97%) and fluorescein isothiocyanate (FITC) were purchased from Sigma-Aldrich (USA). (N)-N-dicyclohexylcarbodiimide (DCC) was purchased from China Pharmaceutical Group Chemical Reagent Co., Ltd. (Shanghai, China). N-hydroxysuccinimide (NHS, purity 98%) was purchased from Aladdin Industrial Corporation. Triethylamine (TEA) was purchased from Tianjin Fuyu Chemical Co., Ltd. Folic acid-free RPMI 1640 medium was obtained from Gibco (NY, USA). RPMI 1640 medium and penicillin/streptomycin were purchased from HyClone (LA, USA). Fetal bovine serum (FBS) was purchased from Biological Industries (Israel). Hoechst 33342 fluorescent dye was obtained from Beyotime Biotechnology (Shanghai, China). MTT, AO/EB, and DAPI were purchased from Beijing Solarbio Science & Technology Co., Ltd. Annexin V-FITC/PI apoptosis detection kit was obtained from KeyGEN Biotech. Co., Ltd. (Nanjing, China). DiR was

purchased from Biotium Inc. (USA). All aqueous solutions were prepared using ultrapure water (Millipore, India).

Preparation of Rg5-BSA NPs

The Rg5-BSA NPs were prepared via the desolvation method as discussed previously.[18] In brief, 45 mg BSA was dissolved in 3 mL water, and the pH was adjusted to 9. The BSA-water mixture was sonicated for 15 mins and stirred for 10 mins at room temperature. Then, 10 mg Rg5 was precisely weighed, dissolved in 1 mL ethanol and added dropwise to the BSA solution. The mixture was stirred for 30 mins at 600 rpm. Eleven milliliters ethanol was continuously added at a rate of 1.5–2.0 mL/min until the mixture appeared turbid. After 24 hrs, the ethanol was removed by evaporation at 40 °C. To obtain pellets, the solution was centrifuged at 12,000 rpm for 30 mins and washed to remove the unencapsulated drug. Finally, the nanoparticles were lyophilized to obtain a white powder for further characterization.

Preparation of FA-Rg5-BSA NPs

First, N-hydroxy succinimide ester of FA (FA-NHS) was prepared according to the method of Lee and Low (1994).[24] Briefly, 1 g FA was dissolved in 20 mL DMSO plus 0.5 mL TEA and reacted with NHS (0.52 g) in the presence of DCC (0.94 g) under stirring in the dark. Afterwards, the solution was filtered, precipitated, centrifuged, and dried, and a yellow powder was obtained.

The modification process of Rg5-BSA NPs with FA was as follows: FA-NHS (6 mg) was dissolved in 1 mL of a carbonate/bicarbonate buffer solution (0.2 M, pH 10), then slowly added dropwise to the Rg5-BSA NPs suspension (3 mL, pH 10) while stirring for 6 hrs in the dark. The suspension was centrifuged (10,000 r/min, 30 mins) and washed. The pellets were redispersed to obtain FA-Rg5-BSA NPs. For blank BSA NPs and FA-BSA NPs, the abovementioned procedure was followed, except for the addition of Rg5.

Determination of the FA amount in FA-Rg5-BSA NPs

The amount of FA modified on Rg5-BSA NPs was determined by UV-vis spectrophotometry.[26] Briefly, the lyophilized FA-Rg5-BSA NPs were hydrolyzed by trypsin under stirring at 37 °C for 2 hrs, then centrifuged at 6000 rpm for 10 mins and scanned in the 250–450 nm range, using the trypsin-hydrolyzed Rg5-BSA NPs and BSA NPs as blank controls. The FA amount in FA-Rg5-BSA NPs was determined at 366 nm using a calibration curve constructed with an FA-NHS solution: $y = 0.0161x + 0.0039$, $R^2 = 0.9998$ (y: absorption; x: FA-NHS concentration, μg/mL).

Entrapment efficiency (EE) and drug loading (DL)

To assess ginsenoside Rg5 entrapment and loading in Rg5-BSA NPs and FA-Rg5-BSA NPs, the NPs were accurately weighed and dissolved in acetonitrile, sonicated for 15 mins to extract the drug completely and then centrifuged at 5000 rpm for 10 mins. Rg5 in the supernatant was then filtered using a 0.45 μm syringe filter and injected into an Agilent 1260 reversed-phase high-pressure liquid chromatography (HPLC) system equipped with an Eclipse Plus C18 column (4.60 mm×250 mm, 5 μm) (Agilent, USA).[27] The mobile phase consisted of HPLC grade water and acetonitrile (50:50% v/v) at a flow rate of 1.5 mL/min. The ultraviolet detection wavelength was set at 203 nm, and the column temperature was maintained at 35 °C. The linear regression equation of the calibration curve for Rg5 over the tested range of 5–100 μg/mL was $y = 4.3124x + 4.1772$, $R^2 = 0.9997$ (y: the peak area; x: Rg5 concentration, μg/mL). Finally, the drug loading (DL) and entrapment efficiency (EE) were calculated using the following equations:

$$\mathrm{DL}(\%) = \frac{\text{weight of Rg5 in nanoparticles}}{\text{weight of nanoparticles}} \times 100\%$$

$$\mathrm{EE}(\%) = \frac{\text{Weight of Rg5 in nanoparticles}}{\text{weight of the feeding Rg5}} \times 100\%$$

Physicochemical characterization of FA-Rg5-BSA NPs

The particle size, polydispersity index (PDI) and zeta potential of Rg5-BSA NPs and FA-Rg5-BSA NPs were measured by a Malvern ZetaSizer Nano ZS analyzer (Nano-ZS ZEN3600, Malvern, UK). The shape and surface morphology of the Rg5-BSA NPs and FA-Rg5-BSA NPs were observed by scanning electron microscopy (SEM, Carl Zeiss ULTRA PLUS) and transmission electron microscopy (TEM, JEM-1230, Japan). The structural characterization of the Rg5-BSA NPs and FA-Rg5-BSA NPs was confirmed by Fourier transform infrared (FT-IR) spectroscopy and nuclear magnetic resonance (^{1}H NMR). The stability of the Rg5-BSA NPs and FA-Rg5-BSA NPs was evaluated by monitoring their size, PDI and count rates in water at 4 °C over time.[28] In order to evaluate the

stability of Rg5-BSA NPs and FA-Rg5-BSA NPs in plasma (ex vivo), these NPs were resuspended in FBS and incubated at 4 °C for 5 days. The particle size of NPs was measured by DLS every day. The thermal stability of Rg5-BSA NPs and FA-Rg5-BSA NPs was investigated by thermogravimetric (TG) analysis and differential scanning calorimetry (DSC) (Shimadzu, Kyoto, Japan). The samples were accurately weighed, placed into standard aluminum pans and carefully sealed. An empty aluminum pan was used as reference. The sample and reference cell were purged with dry nitrogen gas (50 mL/min). For TG analysis, the samples were heated from 50 °C to 700 °C at a constant rate of 10 °C/min. For DSC analysis, the thermograms were obtained at a scanning rate of 10 °C/min over a temperature range of 30 °C −500 °C.[29]

In vitro drug release

The in vitro drug release of Rg5 from the Rg5-BSA NPs and FA-Rg5-BSA NPs was assessed using a membrane dialysis method in neutral medium with PBS (pH 7.4) and in acidic medium with acetate buffer (pH 5.0), respectively, containing 0.5% (v/v) Tween 80 over 140 hrs.[30] In brief, 2 mL Rg5-BSA NPs and FA-Rg5-BSA NPs suspensions (5 mg/mL, 2 mL) were transferred into dialysis bags (MWCO 3500 Da) and then immersed in 50 mL tubes containing 40 mL release medium. The tubes were placed in an orbital water bath shaker at 37.0±0.5 °C with shaking at 120 rpm. At regular time points (0, 3, 6, 12, 24, 36, 48, 60, 72, 96, 120, and 144 h), 5 mL of the release medium was withdrawn and replaced with an equal amount of fresh release medium. The cumulative release percentage of Rg5 from the dialysis bags was determined by HPLC.

Cell culture

Human breast cancer cells (MCF-7) (folate receptor positive tumor cells line), and normal fibroblast cells (L929) (folate receptor negative tumor cells line) were used in this study. They were obtained from the American Type Culture Collection (ATCC, Manassas, VA, USA). The cell lines were cultured in RPMI 1640 culture medium or folic acid-free RPMI 1640 supplemented with 10% FBS and 1% penicillin/streptomycin in a 5% CO_2 atmosphere incubator at 37 °C.

Cell viability assay

The cell viability of Rg5, Rg5-BSA NPs and FA-Rg5-BSA NPs was measured by MTT assay. MTT assay is described in Supplementary materials. The 50% inhibitory concentration (IC_{50}) was calculated using SPSS software. In addition, the cell viability of the blank nanoparticles was tested. Cell viability was calculated by the following equation:

$$\text{Cell Viability}(\%) = \frac{A_{\text{sample}} - A_{\text{blank}}}{A_{\text{Control}} - A_{\text{blank}}} \times 100\%$$

where A_{sample} is the absorbance of the cells incubated with the samples, A_{control} is the absorbance of the cells incubated with the culture medium only (positive control), and A_{blank} is the absorbance of the culture medium without cells (negative control).

Cell apoptosis assay

The apoptotic morphological characteristics of MCF-7 cells treated with Rg5, Rg5-BSA NPs and FA-Rg5-BSA NPs were analyzed by Hoechst 33342 and AO/EB staining. The staining assay is described in Supplementary materials. For the quantitative apoptosis analysis, the MCF-7 cells were treated with 50 μM Rg5, Rg5-BSA NPs and FA-Rg5-BSA NPs, and the culture medium, BSA NPs, and FA-BSA NPs were incubated as controls. Next, the cells were harvested and washed with cold PBS. Then, the cells were resuspended in 100 μL binding buffer containing 5 μL Annexin V-FITC and 5 μL PI. The stained cells were analyzed via flow cytometry.

Cellular uptake assay

FITC was used as the fluorescent marker for labeling the nanoparticles to observe cellular uptake in MCF-7 cells by confocal laser scanning microscopy (CLSM).[31] For quantitative cellular uptake analysis, flow cytometry (FACSCalibur, BD, USA) was utilized to quantify the fluorescence intensity. The confocal laser scanning microscopy and flow cytometry analysis procedures are given in Supplementary materials.

Human breast cancer xenograft mouse model

To examine the in vivo antitumor effect of Rg5-BSA NPs and FA-Rg5-BSA NPs, human MCF-7 breast cancer subcutaneous tumor xenograft mice models were established.[11] The tumor volume was calculated using the formula: Tumor volume (mm^3) = (length) × $(\text{width})^2 \times 0.5$. The establishment process of the human breast cancer xenograft mouse model is given in Supplementary materials.

In vivo imaging of DiR-labeled FA-Rg5-BSA NPs

The in vivo biological distribution of DiR-labeled Rg5-BSA NPs and FA-Rg5-BSA NPs over time was investigated by a near-infrared fluorescence imaging system in MCF-7 tumor-bearing mice.[32,33] A 100 μL portion of free DiR and DiR-labeled nanoparticles was intraperitoneally (i.p.) injected at a dose of 0.5 mg/kg. After injection, fluorescence images were taken at different intervals (2, 8 and 24 h) using an in vivo imaging system (IVIS® Lumina XR Series III, PerkinElmer, Waltham, MA, USA).

Statistical analysis

All data are presented as the mean ± SD. Statistical analysis of the data was conducted by one-way ANOVA for more than two groups and Student's *t*-test for two groups utilizing SPSS software (version 19.0). A difference was considered significant when $p<0.05$ and highly significant when $p<0.01$.

Results and discussion

Preparation of Rg5-BSA NPs and Fa-Rg5-Bsa Nps

BSA has been extensively used as a delivery carrier for drug. A schematic illustration for the preparation of FA-Rg5-BSA NPs is given in Figure 1, Rg5-loaded nanoparticles are prepared using desolvation method, which is a simple and economic pathway for drug encapsulation of albumin-based nanoparticles. This method often has a narrow particle size distribution and a low polydispersity index (PDI). BSA was dispersed in water and the pH was adjusted to be alkaline and ethanol was used as the dehydrating agent. The preparation of Rg5-BSA NPs was based on the differential solubility of BSA in different solvents, namely, the high solubility in water and low solubility in ethanol, which removed the hydrated membrane of BSA to produce nanoparticles with the addition of ethanol.[18]

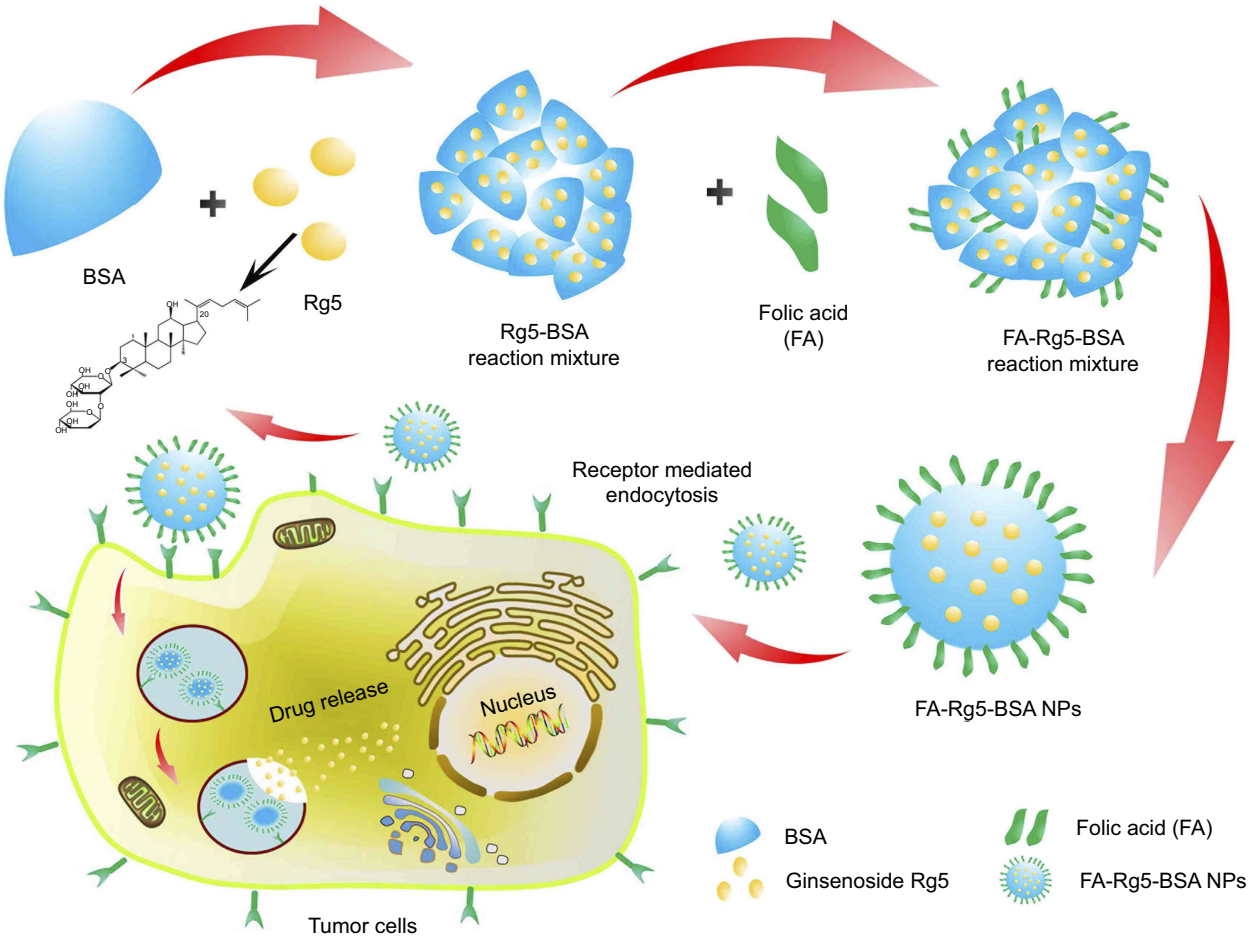

Figure 1 Schematic illustration of preparation of FA-Rg5-BSA NPs.
Abbreviations: BSA, bovine serum albumin; Rg5, ginsenoside Rg5; FA, folic acid; NPs, nanoparticles.

The organic solvent removed by evaporation, and then Rg5-loaded nanoparticles were collected by centrifugation.

FA was further modified on the surface of Rg5-BSA NPs by means of a simple amide bond. The various parameters of the preparation process were optimized, such as the concentration and pH of BSA, water-ethanol ratio, ratio of raw materials, rate of adding ethanol, and solution stirring time, to ensure the desired particle size and drug loading ability. The optimization results of Rg5-BSA NPs and FA-Rg5-BSA NPs are summarized in Supplementary materials (Tables S1-S10). The mean particle size ranged from 154.4 to 321.4, and it was mainly influenced by pH value of BSA solution and volume ratio of ethanol to water. Similar findings were reported by Li et al indicated that the pH and the amount of ethanol exert a considerable impact on the formation of BSA nanoparticles.[34] Therefore, the parameters (pH 9, ethanol to water volume ratio of 3:1) were set to obtain the desired particle size and encapsulation efficiency. Albumin has an augmented viscosity and decreased dissolvability at pH 9, which facilitate its preparation into nanoparticles.[34] The modification of FA on the surface of Rg5-BSA NPs (Rg5 to BSA molar ratio of 20:1) had the minimum particle size (233.6 nm) when folic acid to BSA molar ratio of 15:1.

Particle size and size distribution properties play a vital role in the stability, cellular uptake and drug release. Typically, the size of the NPs less than 400 nm accumulate preferentially in tumor tissue rather than in normal tissues. This result appears to be a consequence of the enhanced permeability and retention (EPR) effect.[21] In Figure 2A and B, the resulting optimized Rg5-BSA NPs and FA-Rg5-BSA NPs had average hydrodynamic sizes of 164.0 nm and 201.4 nm, respectively, which indicated uniform and narrow particle size distributions.[29,35] After the modification of FA on the surface of Rg5-BSA NPs increased the size of particles. Surface morphology and particle size of the Rg5-BSA NPs and FA-Rg5-BSA NPs were examined by SEM and TEM. The Rg5-BSA NPs and FA-Rg5-BSA NPs were nearly monodisperse spheres with smooth surfaces (Figure 2C and D). Folic acid attached to the surface of Rg5-BSA NPs was not visible by SEM and TEM. Moreover, the particle size was slightly smaller than that of DLS result because of lack of hydration shell when particle size was determined by SEM and TEM.[31] Zeta potential serves as an indicator of surface charge, which mainly affects the stability of the nanoparticles in dispersion. The higher the absolute value of the zeta potential, the higher the surface charge of the NPs. The FA modification to the Rg5-BSA NPs increased the negative surface charge of Rg5-BSA NPs from −14.9 mV to −22.5 mV, since the content of free amino groups decreased after FA modification. The zeta potential values of Rg5-BSA NPs and FA-Rg5-BSA NPs were negative, which increased when the NPs entered a weakly acidic tumor environment. As a result, the stability of the nanoparticles decreased, consequently triggering the release of Rg5.

An absorption peak at 366 nm appeared for FA-NHS as well as for the trypsin-hydrolyzed product of FA-Rg5-BSA NPs, while this absorption peak did not appear for trypsin-hydrolyzed Rg5-BSA NPs and BSA NPs (Figure 2E), which indicated that FA was modified on the surface of Rg5-BSA NPs. In addition, the amount of FA in FA-Rg5-BSA NPs was 94.6 μg/mg BSA NPs according to the calibration curve.[36,37] The entrapment efficiency (EE) of the Rg5-BSA NPs and FA-Rg5-BSA NPs is summarized in Table 1. The drug loading (DL) of the Rg5-BSA NPs and FA-Rg5-BSA NPs was optimized to be 14.53±2.63%, and 12.64±4.02%, respectively. It could be seen that Rg5-BSA NPs achieved a higher drug EE and DL. The slight decrease in the drug loading in FA-Rg5-BSA NPs was attributed to loss of drug during the process of modification of FA on the surface of Rg5-BSA NPs.

Characterization of folic acid modification

The FA-Rg5-BSA NPs were prepared by conjugating FA to the amino groups of Rg5-BSA NPs to form an amide linkage, which was proved by FT-IR and ^{1}H NMR. Figure 3A displayed a comparison of the FT-IR spectra of BSA, Rg5, FA, Rg5-BSA NPs, and FA-Rg5-BSA NPs. The peaks at approximately 1063.38 cm^{-1} for the Rg5-BSA NPs and at 1028.79 cm^{-1} for the FA-Rg5-BSA NPs corresponded to the characteristic peak (C=O) of the Rg5 molecule at 1069.36 cm^{-1}. The appearance of a peak at 1450.49 cm^{-1} for the FA-Rg5-BSA NPs corresponded to the phenyl ring of folic acid, and the new characteristic peaks at 1606.80 and 1537.63 cm^{-1} belonged to the amide linkage. These results preliminarily determined that Rg5 was encapsulated and that FA was conjugated.[38] In Figure 3B, the ^{1}H NMR spectra of Rg5-BSA NPs and FA-Rg5-BSA NPs exhibited the characteristic peaks of the Rg5 at approximately 0.88–1.50 ppm, and the characteristic peaks of the aromatic protons for FA at

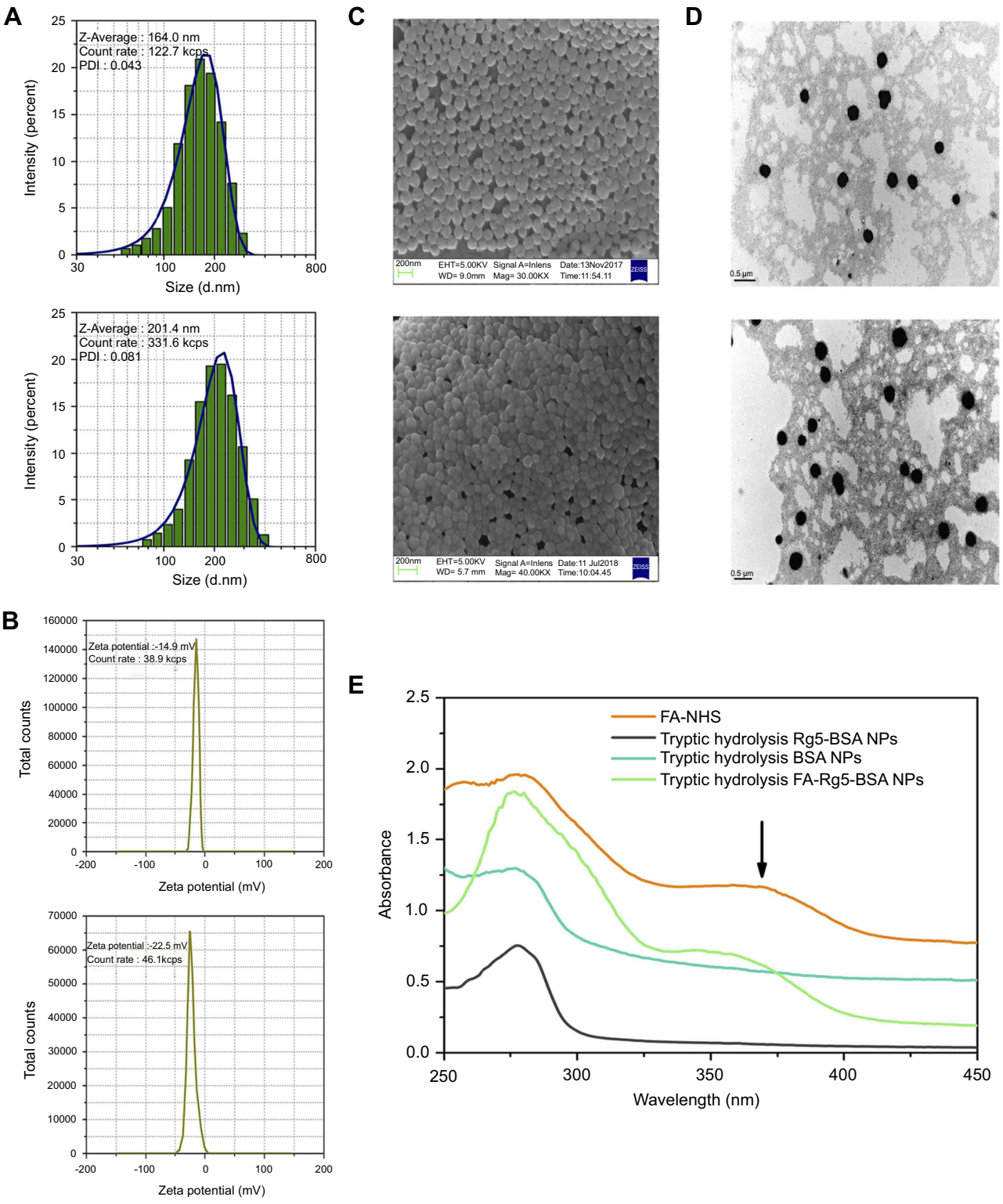

Figure 2 (**A**) Hydrodynamic size distributions, (**B**) Zeta potentials, (**C**) SEM and (**D**) TEM images of Rg5-BSA NPs (top) and FA-Rg5-BSA NPs (bottom), and (**E**) UV-vis absorption spectra determining the amount of FA in Rg5-BSA NPs.

Abbreviations: BSA, bovine serum albumin; Rg5, ginsenoside Rg5; FA, folic acid; NPs, nanoparticles; SEM, scanning electron microscopy; TEM, transmission electron microscopy.

7.88 ppm, 7.66 ppm, and 6.65 ppm were present for the FA-Rg5-BSA NPs, further confirming the effective encapsulation of Rg5 in the particles, as well as the successful FA modification to the Rg5-BSA NPs.[39,40]

Table 1 Key parameters of Rg5-BSA NPs and FA-Rg5-BSA NPs

Samples	Particle size (nm)	PDI	Zeta potential (mV)	Entrapment efficiency (%)	Drug loading (%)	The amount of FA (μg/mg BSA NPs)
Rg5-BSA NPs	164.0±3.6	0.043±0.039	−14.9±1.7	78.26±5.42	14.53±2.63	–
FA-Rg5-BSA NPs	201.4±2.9	0.081±0.064	−22.5±2.6	73.59±5.50	12.64±4.02	94.6±17.5

Notes: Data are represented as mean ± SD, n=3.
Abbreviations: BSA, bovine serum albumin; Rg5, ginsenoside Rg5; FA, folic acid; NPs, nanoparticles; PDI, polydispersity index.

Physicochemical properties of Rg5-BSA NPs and FA-Rg5-BSA NPs

The stability of nanoparticles not only facilitates the transportation and storage of the drug but also helps the drug reach the cells efficiently. As shown in Figure 4, the Rg5-BSA NPs and FA-Rg5-BSA NPs aqueous solutions were visually no precipitation throughout the observation period. In addition, the particle size, PDI and count rates of Rg5-BSA NPs and FA-Rg5-BSA NPs showed no drastic change. The stability of Rg5-BSA NPs and FA-Rg5-BSA NPs was maintain for 8 weeks at 4 °C.

The stability of Rg5-BSA NPs and FA-Rg5-BSA NPs in plasma (ex vivo) was monitored by DLS. The result was shown in Figure S1 in Supplementary materials, it can be seen that Rg5-loaded nanoparticles show an excellent stability in FBS.

Additionally, the thermal properties of Rg5-BSA NPs and FA-Rg5-BSA NPs were analyzed by TG analysis and DSC. Compared to that of Rg5, the degradation rate of FA-Rg5-BSA NPs was slow, suggesting that FA-Rg5-BSA NPs had better stability over a wide range of temperatures. These data are shown in Figures S2 and S3 in Supplementary materials.

In vitro drug release

The in vitro drug release profile of Rg5 from the Rg5-BSA NPs and FA-Rg5-BSA NPs over 140 hrs was shown in Figure 5. The release of Rg5 exhibited a pH-dependent manner, the release rate of Rg5 at pH 5.0 was significantly faster than that at pH 7.4. At pH 5.0, the cumulative release percentage of Rg5 reached 46.20±3.44% for the FA-Rg5-BSA NPs in the first 48 hrs, then increased to 86.29±3.87% from the 48th to the 96th hour, showing almost complete drug release. A similar release profile was also observed for the Rg5-BSA NPs. At pH 7.4, only about half of Rg5 was released for Rg5-BSA NPs and FA-Rg5-BSA NPs within 144 hrs, which revealed slow and sustained drug release. Because the BSA carrier was susceptible to erosion and degradation in acidic environments which coincides with the pH of tumor microenvironment, the release of Rg5 from the nanoparticles was faster in cancer tissues than in normal cells. In this way, nanoparticles could continuously and effectively inhibit the growth of cancer cells.[41,42]

In vitro viability assay

It is necessary to evaluate the cytotoxicity of the nanocarrier before further biomedical applications.[43,44] The results in Figure 6A and B demonstrated that the empty BSA NPs and FA-BSA NPs did not exhibit any significant toxicity toward the MCF-7 and L929 cells for 72 hrs. To assess the inhibitory effect on cancer cells and normal cells, MCF7 cells and L929 cells treated with Rg5, Rg5-BSA NPs and FA-Rg5-BSA NPs for 24 hrs and 48 hrs by means of the MTT assay.[40,45–47] As shown in Figure 6C–F, the effect of Rg5, Rg5-BSA NPs and FA-Rg5-BSA NPs on both cell lines showed dose-and time-dependent behavior. The IC_{50} value of Rg5, Rg5-BSA NPs and FA-Rg5-BSA NPs in the MCF-7 and L929 cells were shown in Table 2. The IC_{50} value of Rg5-BSA NPs and FA-Rg5-BSA NPs were similar in the L929 cells (higher than the IC_{50} of Rg5) and 3 or 4 times higher than that in the MCF-7 cells (lower than the IC_{50} of Rg5). Compared with Rg5, the Rg5-BSA NPs and FA-Rg5-BSA NPs had superior anticancer activity in MCF-7 cells and minor effect in L929 cells due to the selectivity of nanoparticles and the biocompatible nature of BSA. In addition, the difference in the IC_{50} of FA-Rg5-BSA NPs between the L929 cells and the MCF-7 cells was greater than that of Rg5-BSA NPs, indicating that FA-Rg5-BSA NPs had the best anticancer activity in MCF-7 cells. Due to the highly expressed FA receptors in MCF-7 cells, FA-Rg5-BSA NPs might be internalized into the cells by receptor-mediated endocytosis with the specific ligand-receptor interaction. Consequently, the enhanced internalization of FA-Rg5-BSA NPs resulted in the accumulation of intracellular Rg5, further achieving significant cytotoxicity in the MCF-7 cells.

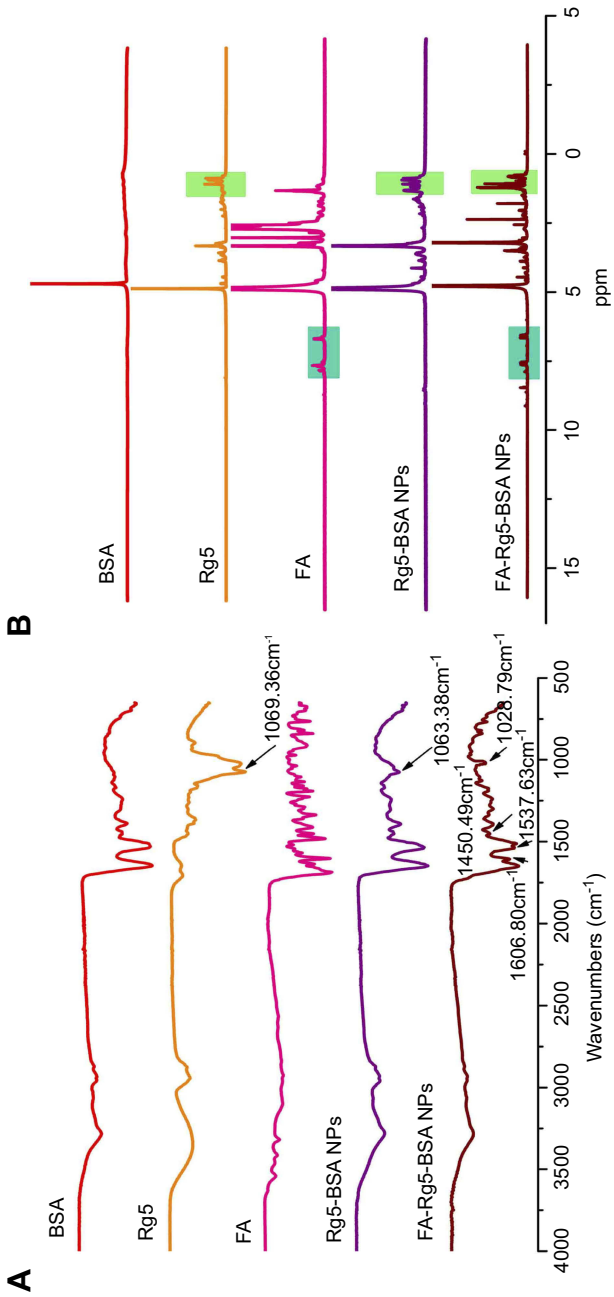

Figure 3 Characterization of folic acid modification.
Notes: (**A**) The FT-IR and (**B**) ^{1}H NMR spectra of BSA, Rg5, FA, Rg5-BSA NPs and FA-Rg5-BSA NPs.
Abbreviations: BSA, bovine serum albumin; Rg5, ginsenoside Rg5; FA, folic acid; NPs, nanoparticles; FT-IR, fourier transform infrared spectroscopy; ^{1}H NMR, nuclear magnetic resonance.

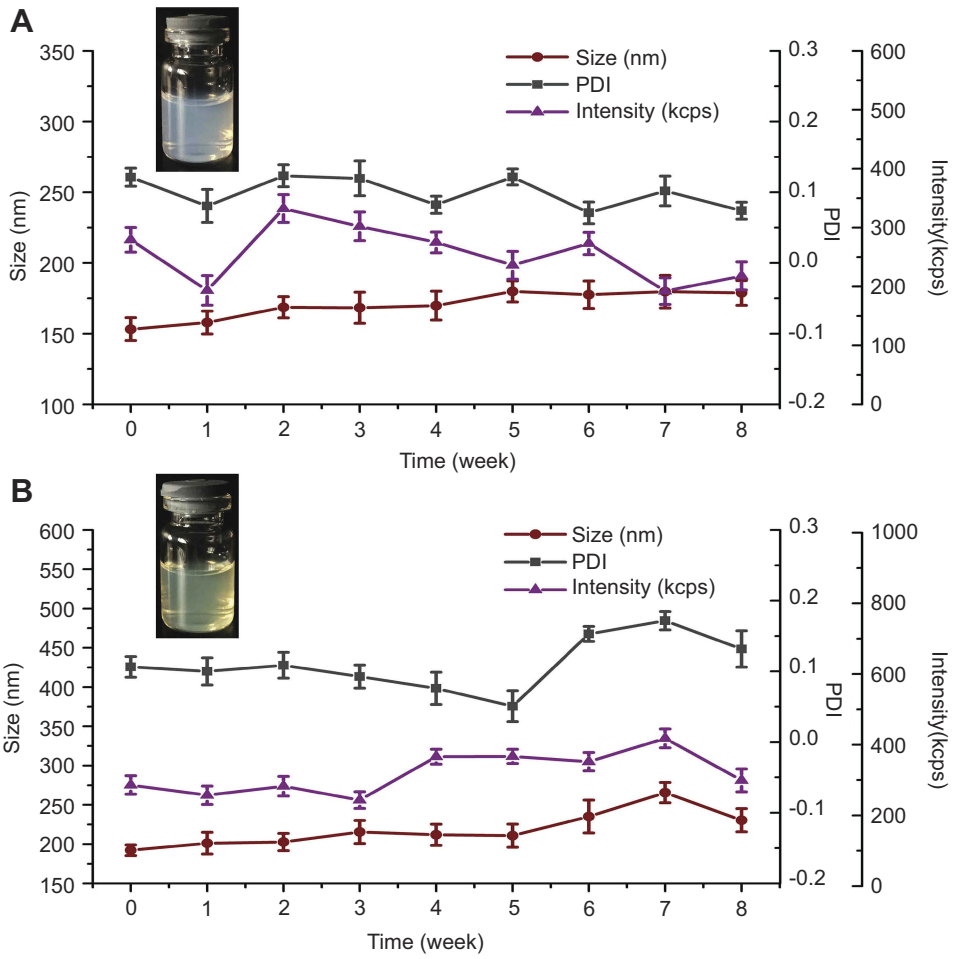

Figure 4 The stability of Rg5-BSA NPs and FA-Rg5-BSA NPs over time.
Notes: The stability of Rg5-BSA NPs (**A**) and FA-Rg5-BSA NPs (**B**) in water at 4 °C for 8 weeks. Data are represented as mean ± SD, n=3.
Abbreviations: BSA, bovine serum albumin; Rg5, ginsenoside Rg5; FA, folic acid; NPs, nanoparticles; PDI, polydispersity index.

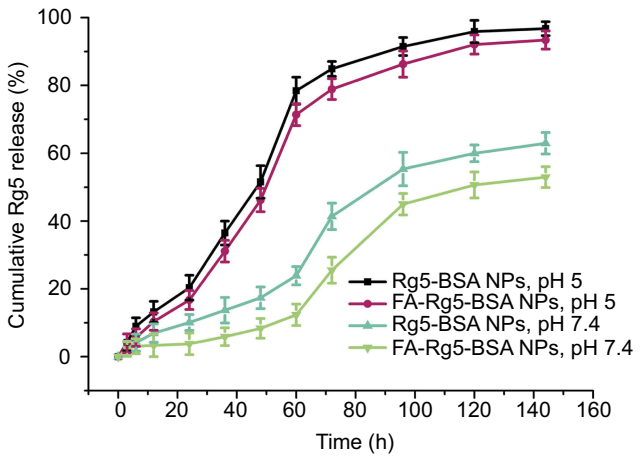

Figure 5 The release curve of Rg5 from Rg5-BSA NPs and FA-Rg5-BSA NPs.
Notes: The in vitro cumulative release percentage of Rg5 from Rg5-BSA NPs and FA-Rg5-BSA NPs over 140 hrs at different pH values (pH 5 and 7.4).
Abbreviations: BSA, bovine serum albumin; Rg5, ginsenoside Rg5; FA, folic acid; NPs, nanoparticles.

Qualitative and quantitative cell apoptosis assays

To identify whether or not the inhibitory effect was associated with the induction of apoptosis, the apoptosis of MCF-7 cells treated with Rg5, Rg5-BSA NPs and FA-Rg5-BSA NPs was analyzed by Hoechst 33342 staining, AO/EB staining, and Annexin V-FITC/PI dual staining. As shown in Figure 7A, Hoechst 33342 staining demonstrated that the nuclei of untreated cells displayed a pale blue fluorescence. Nevertheless, the luminous blue fluorescence of the Rg5, Rg5-BSA NPs and FA-Rg5-BSA NPs groups gradually increased, indicating that the apoptotic cells in the FA-Rg5-BSA NPs group were more obvious than those in the Rg5 and Rg5-BSA NPs groups. Notably, the AO/EB staining results demonstrated that the FA-Rg5-BSA NPs group had the largest

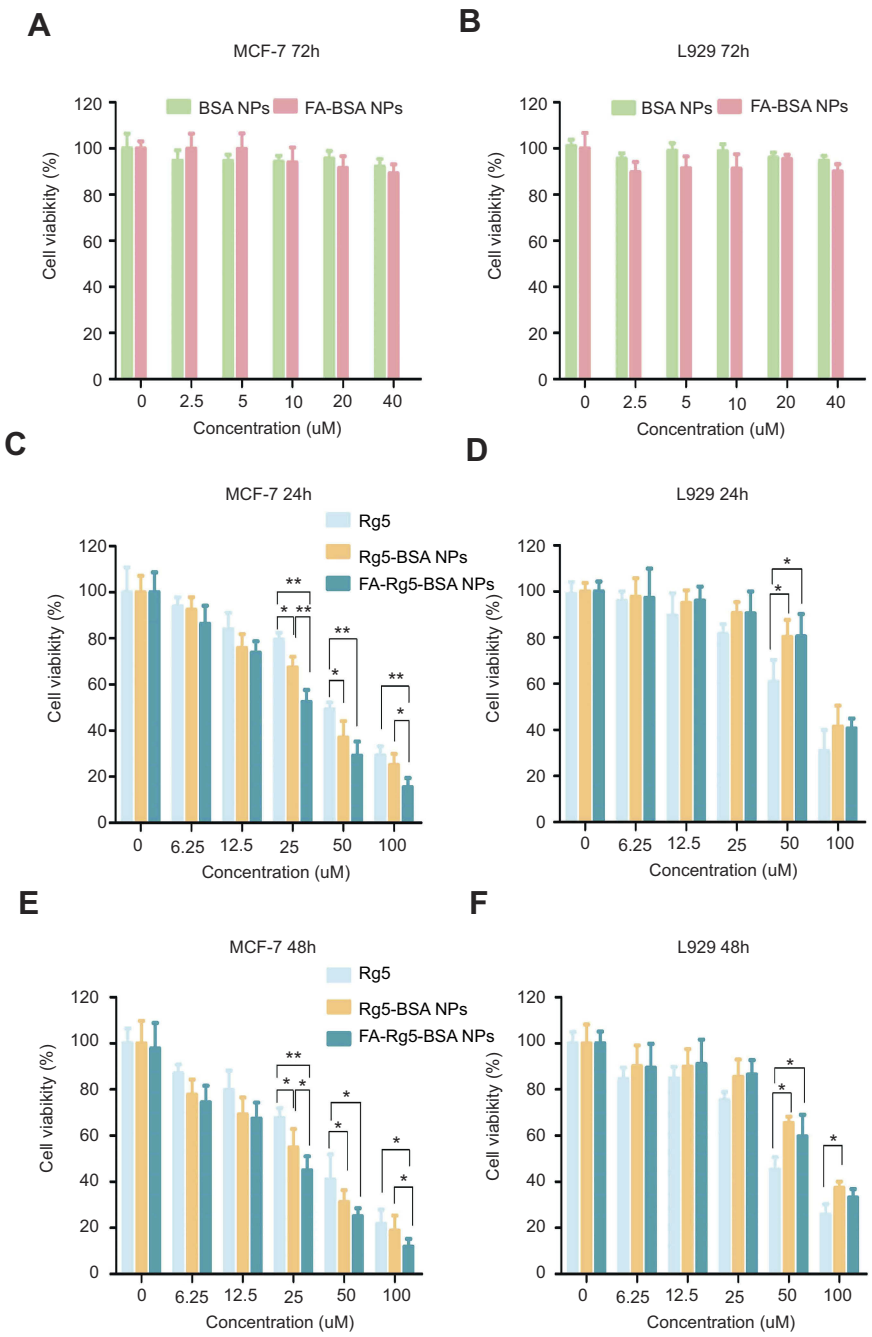

Figure 6 In vitro cell viability assay.
Notes: Cell viability of blank BSA NPs, FA-BSA NPs against MCF-7 cells (**A**) and L929 cells (**B**) after incubating for 72 hrs; cell toxicity of Rg5, Rg5-BSA NPs and FA-Rg5-BSA NPs against MCF-7 cells (**C, E**) and L929 cells (**D, F**) for 24 hrs and 48 hrs. Values are represented as mean ± SD. (n=3, *P<0.05, **P<0.01).
Abbreviations: BSA, bovine serum albumin; Rg5, ginsenoside Rg5; FA, folic acid; NPs, nanoparticles.

number of dead cells, with the maximum amount of red fluorescence. To further confirm these results, Annexin V-FITC/PI staining was carried out to quantify the cell apoptosis rate, as shown in Figure 7B.[48] The percentage of apoptotic cells (early apoptotic plus late apoptotic cells) was approximately 33.10±2.57% for FA-Rg5-BSA NPs, 18.39±2.04% for Rg5-BSA NPs, and 11.71±1.68% for Rg5. This result proved that compared to all other groups, the FA-Rg5-BSA NP group could induce high apoptosis in MCF-7 cells.

Table 2 The IC_{50} of Rg5, Rg5-BSA NPs and FA-Rg5-BSA NPs in MCF-7 and L929 cells

Cell lines	Incubation time (hrs)	IC_{50} (μM)		
		Rg5	Rg5-BSA NPs	FA-Rg5-BSA NPs
MCF-7 cells	24 48	52.98±3.76 38.61±7.72	38.28±4.68 25.46±0.28	26.55±0.84 19.75±2.58
L929 cells	24 48	65.02±18.17 46.86±5.55	111.67±32.98 77.74±9.25	102.90±21.81 70.11±7.87

Notes: Data are represented as mean ± SD, n=3.
Abbreviations: BSA, bovine serum albumin; Rg5, ginsenoside Rg5; FA, folic acid; NPs, nanoparticles.

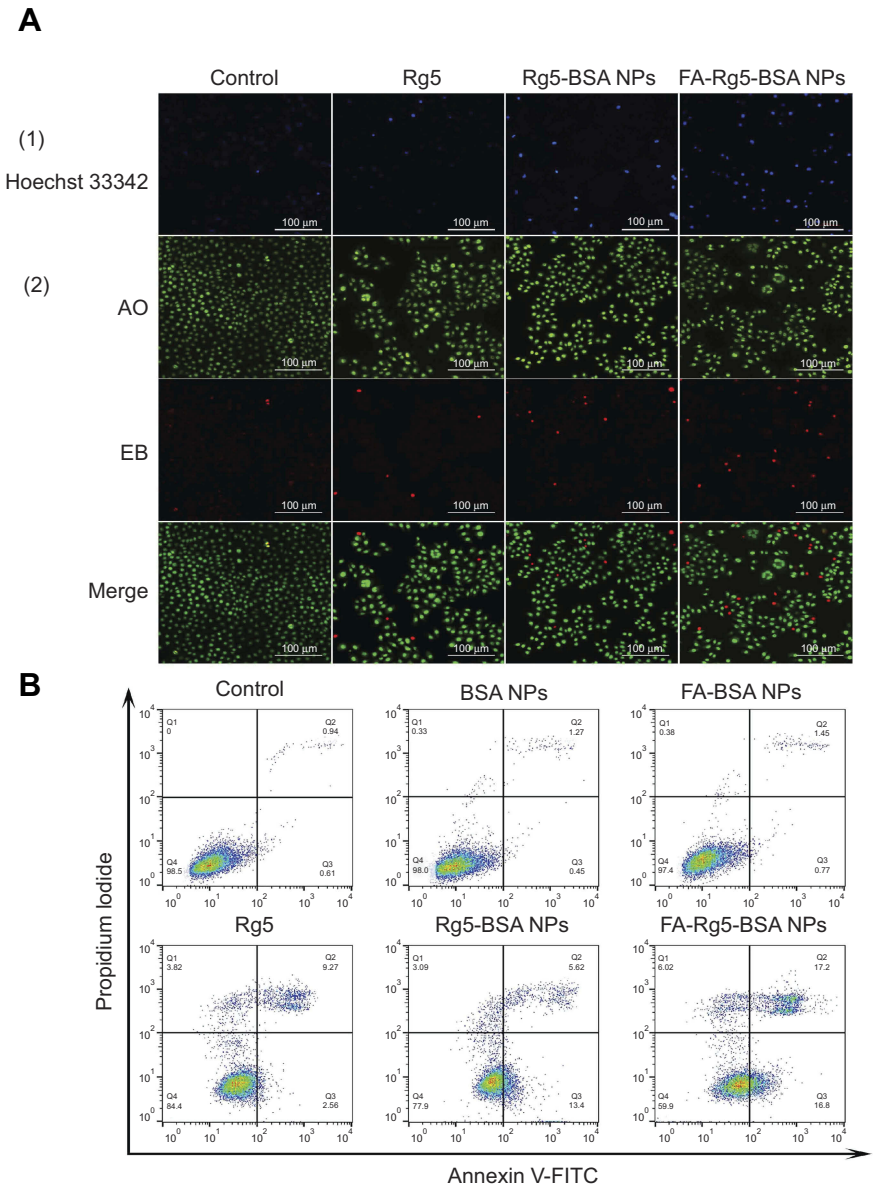

Figure 7 Cell apoptosis assay of MCF-7 cells treated with Rg5, Rg5-BSA NPs and FA-Rg5-BSA NPs by (**A**) Hoechst 33,342, AO/EB, and (**B**) Annexin V-FITC/PI staining.
Note: Magnification 20× and scale bar is 100 μm.
Abbreviations: BSA, bovine serum albumin; Rg5, ginsenoside Rg5; FA, folic acid; NPs, nanoparticles; AO/EB, Acridine orange/ethidium bromide.

Qualitative and quantitative cellular uptake assays

The cellular uptake of FITC-labeled NPs (Rg5-BSA NPs, FA-Rg5-BSA NPs, and FA-Rg5-BSA NPs plus free FA) in MCF-7 cells was observed by CLSM and flow cytometry. FITC-labeled FA-Rg5-BSA NPs displayed the fluorescence intensity of 90.19% (Figure 8B) and most of them were located in the cytoplasm region (Figure 8A). The fluorescence intensity of FITC-labeled FA-Rg5-BSA NPs was much stronger than that of FITC-labeled Rg5-BSA NPs (50.16%), due to the overexpression of FA receptors by MCF-7 cells. More importantly, the addition of free FA clearly decreased the intracellular fluorescence intensity of FITC-labeled FA-Rg5-BSA NPs to 74.54%, suggesting that the cellular uptake of NPs was inhibited by the competitive binding of free FA to FA receptors on the surface of MCF-7 cells. These results demonstrated that the FA molecule modified on the nanoparticles could facilitate

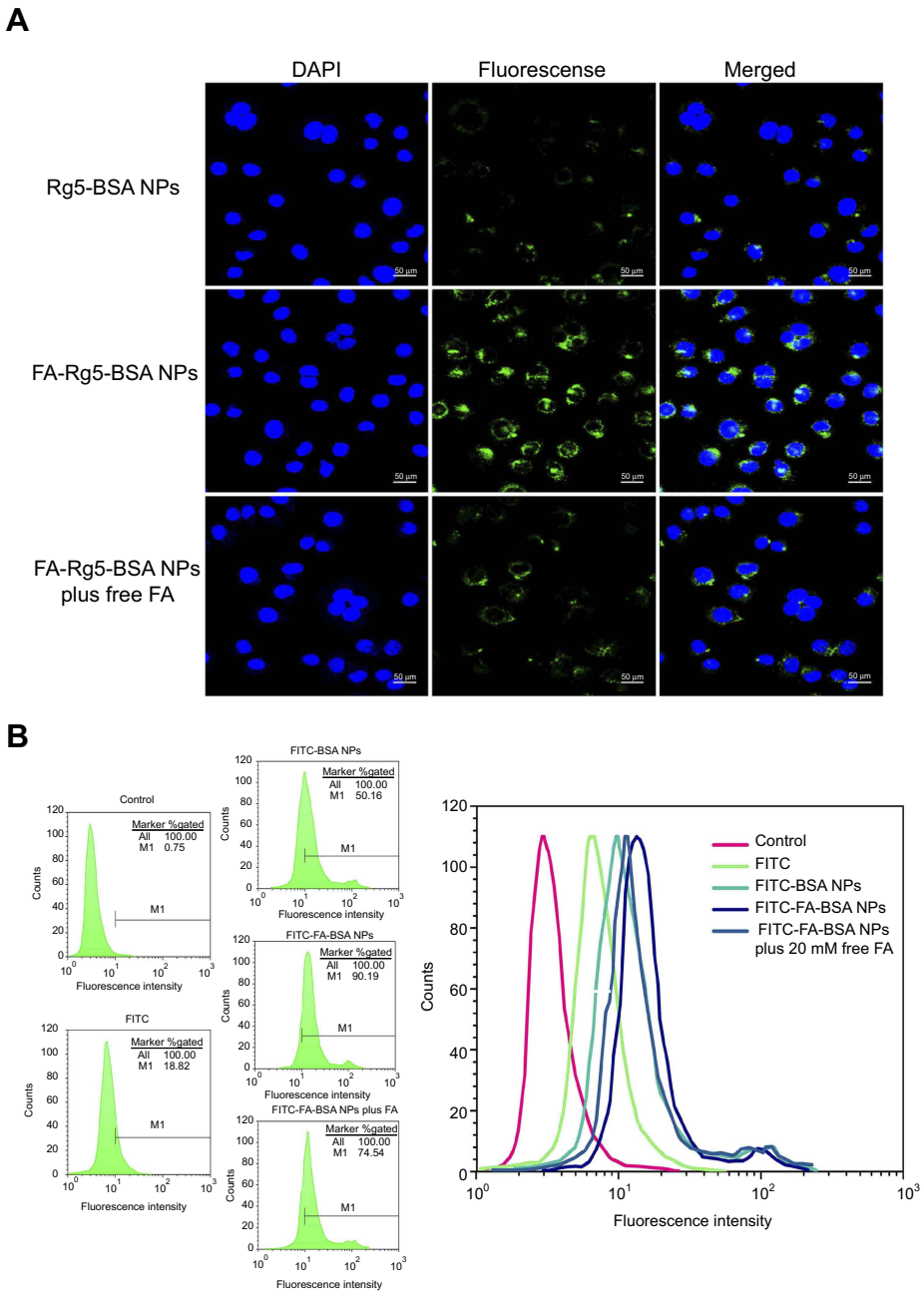

Figure 8 The cellular uptake of FITC-labeled NPs treated with MCF-7 cells for 3 hrs was observed by CLSM (**A**) and flow cytometry (**B**).
Note: Magnification 40× and scale bar is 50 μm.
Abbreviations: BSA, bovine serum albumin; Rg5, ginsenoside Rg5; FA, folic acid; NPs, nanoparticles; FITC, fluorescein isothiocyanate; CLSM, confocal laser scanning microscopy.

and enhance cellular uptake through the FA receptor mediated endocytosis process. Active cellular targeting may be achieved by modifying the surface of Rg5-BSA NPs with FA ligands that accelerate the cellular internalization of nanodrugs, eventually increasing the intracellular Rg5 content.

In vivo antitumor evaluation of FA-Rg5-BSA NPs

The in vivo antitumor effect of Rg5-BSA NPs and FA-Rg5-BSA NPs was evaluated using an MCF-7 tumor-bearing mouse model (Figure 9).[49] Compared to that in the control group, the tumor size of all models in the Rg5-BSA NPs and FA-Rg5-BSA NPs groups was dramatically suppressed due to the antitumor effect of Rg5. At day 21, the average tumor volume in the FA-Rg5-BSA NPs group was 750.85±263.39 mm^3, which was remarkably smaller than that of the Rg5-BSA NPs group (1050.19 ±294.54 mm^3) and the Rg5 group (1350.4±269.91 mm^3). The tumor weight inhibitory rate of the mice was 48.84 ±9.74% for the Rg5 group, 69.91±11.77% for the Rg5-BSA NPs group, and 79.25±6.36% for the FA-Rg5-BSA NPs group. Obviously, the tumor weight inhibitory rate of the FA-Rg5-BSA NPs group was the highest, which was consistent with the tumor volume inhibition rate in nude mice. Significantly, the body weight of the mice was not alleviated by Rg5, Rg5-BSA NPs and FA-Rg5-BSA NPs, similar to that of the control group. This finding indicated that Rg5 probably had minimal side effects on the mice. Hence, the in vivo antitumor activity of FA-Rg5-BSA NPs was more favorable than that of Rg5 and Rg5-BSA NPs.

Imaging the biodistribution of DiR-labeled FA-Rg5-BSA NPs

DiR-labeled Rg5-BSA NPs and FA-Rg5-BSA NPs were utilized to monitor the in vivo real-time biodistribution and the tumor targeting effect of the nanoparticles (Figure 10). In the free DiR group, the fluorescence of DiR was clearly

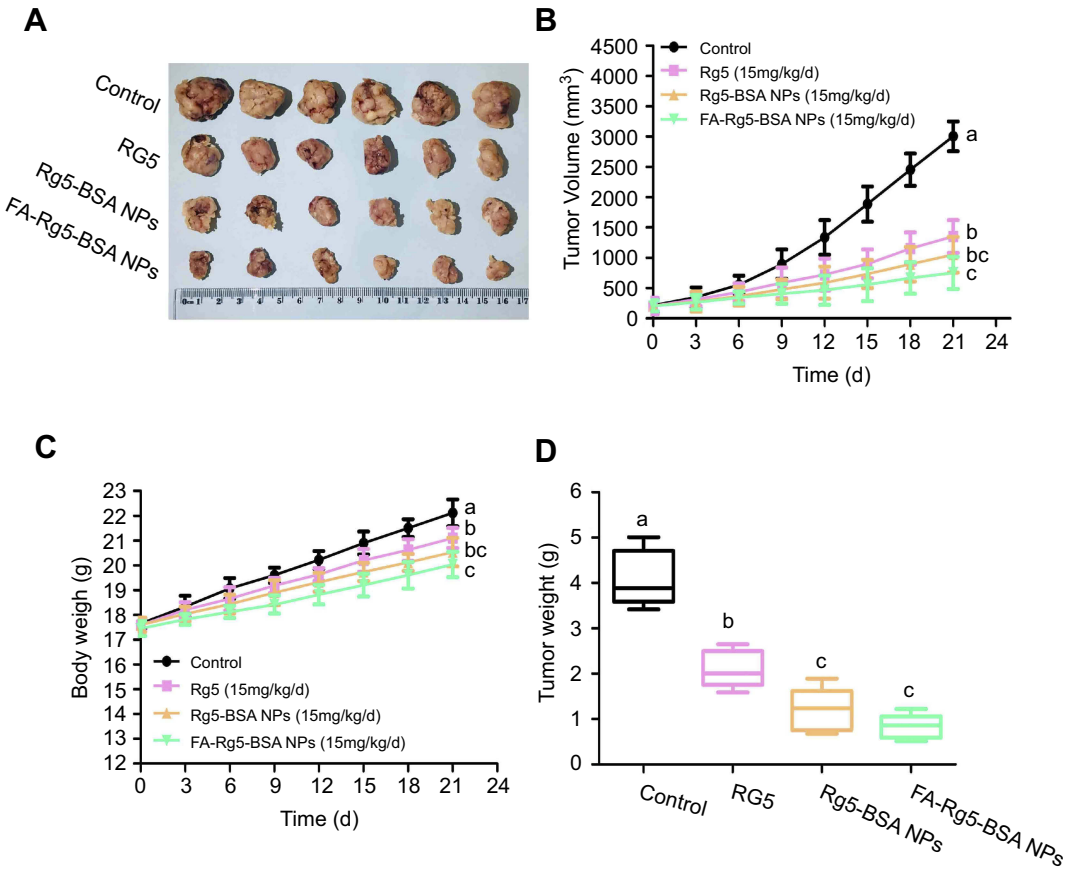

Figure 9 Rg5, Rg5-BSA NPs and FA-Rg5-BSA NPs significantly inhibited the growth of MCF-7 xenograft in vivo.
Notes: (**A**) The image of MCF-7 xenograft tumors with different treatments at 21 days. (**B**) Tumor volume and (**C**) body weight were measured every 3 days. (**D**) Tumor weight after 21 days treatment. $p<0.05$ was considered to have a significant difference. Different letters indicate significant differences between each group.
Abbreviations: BSA, bovine serum albumin; Rg5, ginsenoside Rg5; FA, folic acid; NPs, nanoparticles.

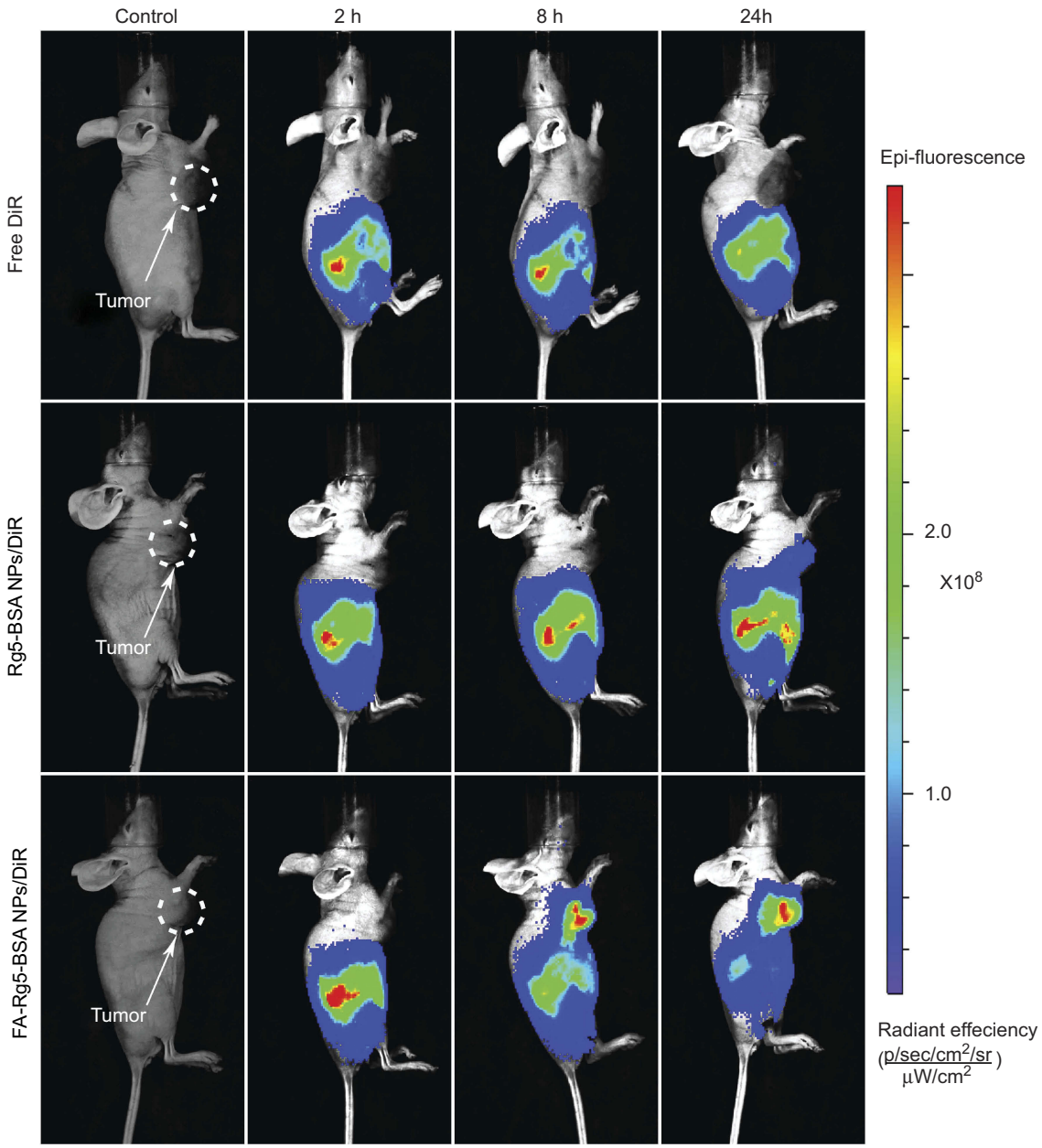

Figure 10 The in vivo real-time biodistribution imaging.
Notes: MCF-7 tumor-bearing mice treated with free DiR, Rg5-BSA NPs/DiR, and FA-Rg5-BSA NPs/DiR at 2 h, 8 h and 24 h.
Abbreviations: BSA, bovine serum albumin; Rg5, ginsenoside Rg5; FA, folic acid; NPs, nanoparticles; DiR, dioctadecyl-tetramethyl indotricarbocyanine iodide.

observed on the abdomen of nude mice at 2 hrs and then quickly declined over time. No fluorescence emerged in the tumor site of the mice. Regarding the Rg5-BSA NPs/DiR group, the body of mice as a whole had pronounced fluorescence. The region of the tumor in nude mice showed faint fluorescence at 24 hrs. Rg5-BSA NPs preferentially accumulate in tumors via a passive targeting mechanism named enhance permeability and retention (EPR) effect. Significantly, for the FA-Rg5-BSA NPs/DiR group, the tumor area of the mice already showed higher fluorescence at 8 hrs than that of the Rg5-BSA NPs/DiR group at 24 hrs. There was much stronger fluorescence at 24 hrs in the tumor position for the FA-Rg5-BSA NPs/DiR group. Thus, FA-Rg5-BSA NPs mainly accumulated in cancerous tissues after 8 hrs, and FA-Rg5-BSA NPs exhibited more powerful tumor targeting ability than that of Rg5-BSA NPs. FA-Rg5-BSA NPs are actively directed towards the cancer cells due to the abundant presence of FA receptors on their surface, causing enhanced uptake and internalization of nanoparticles through receptor-mediated endocytosis.

Conclusion

In conclusion, a promising nanotechnology-based targeted drug delivery system was developed by utilizing BSA as the carrier to entrap Rg5; then, Rg5-BSA NPs was packed with the target molecule FA. The resultant Rg5-loaded NPs showed suitable particle size, uniform spherical shape, and favorable bioactivity. In particular, FA-Rg5-BSA NPs evoked more cytotoxicity than Rg5 in MCF-7 cells but less cytotoxicity in normal L929 cells. In oncology, receptors-mediated endocytosis and the EPR effect are the primary rationales for delivering nanoparticles to cancer cells. Additionally, FA-Rg5-BSA NPs could induce a high level of apoptotic cell death. Moreover, FA-Rg5-BSA NPs was highly taken up by MCF-7 cells. In the MCF-7 xenograft mouse model, FA-modified targeted nanoparticles enabled efficient Rg5 accumulation at the tumor site in 8 hrs. Overall, this targeted Rg5 delivery system offers several appealing advantages, such as improved drug therapeutic effects, intensive selectivity and enhanced ability to target carcinoma cells. Prospectively, a series of Rg5-related nanodrugs for cancer therapy can be continuously explored and further popularized in the future.

Acknowledgments

This study was financially supported by grants from the National Natural Science Foundation of China (21676214, 21808184, and 21878246), the Shaanxi Key Laboratory of Degradable Biomedical Materials Program (2014SZS07-Z01 and 15JS105), and the Shaanxi R&D Center of Biomaterials and Fermentation Engineering Program (2016SZSj-35).

Disclosure

The authors report no conflicts of interest in this work.

References

1. Mun EJ, Babiker HM, Weinberg U, Kirson ED, Von Hoff DD. Tumor-treating fields: a fourth modality in cancer treatment. *Clin Cancer Res*. 2018;24(2):266. doi:10.1158/1078-0432.CCR-17-1117
2. Partridge AH, Elmore JG, Saslow D, McCaskill-Stevens W, Schnitt SJ. Challenges in ductal carcinoma in situ risk communication and decision-making: report from an American Cancer Society and National Cancer Institute workshop. *CA Cancer J Clin*. 2012;62(3):203–210. doi:10.3322/caac.21140
3. Oun R, Moussa YE, Wheate NJ. The side effects of platinum-based chemotherapy drugs: a review for chemists. *Dalton Trans*. 2018;47(19):6645–6653. doi:10.1039/c8dt00838h
4. Tamura T, Miyazaki K, Shiozawa T, Satoh H. Comparative effectiveness and resource usage in patients receiving first-line taxol-based chemotherapy for stage IV NSCLC. *Clin Lung Cancer*. 2018;19(1):e67. doi:10.1016/j.cllc.2017.06.018
5. Duan L, Xiong X, Hu J, Liu Y, Li J, Wang J. Panax notoginseng saponins for treating coronary artery disease: a functional and mechanistic overview. *Front Pharmacol*. 2017;8:702. doi:10.3389/fphar.2017.00702
6. Wang T, Guo R, Zhou G, et al. Traditional uses, botany, phytochemistry, pharmacology and toxicology of Panax notoginseng (Burk.) F. H. Chen: a review. *J Ethnopharmacol*. 2016;188:234–258. doi:10.1016/j.jep.2016.05.005
7. Gillis CN. Panax ginseng pharmacology: a nitric oxide link? *Biochem Pharmacol*. 1997;54(1):1–8. doi:10.1016/s0006-2952(97)00193-7
8. Shin YW, Bae EA, Kim DH. Inhibitory effect of ginsenoside Rg5 and its metabolite ginsenoside Rh3 in an oxazolone-induced mouse chronic dermatitis model. *Arch Pharm Res*. 2006;29(8):685–690.
9. Kim S-J, Kim AK. Anti-breast cancer activity of fine black ginseng (Panax ginseng Meyer) and ginsenoside Rg5. *J Ginseng Res*. 2015;39(2):125–134. doi:10.1016/j.jgr.2014.09.003
10. Li W, Yan M-H, Liu Y, et al. Ginsenoside Rg5 ameliorates cisplatin-induced nephrotoxicity in mice through inhibition of inflammation, oxidative stress, and apoptosis. *Nutrients*. 2016;8(9):566. doi:10.3390/nu8090566
11. Liu Y, Fan D. Ginsenoside Rg5 induces apoptosis and autophagy via the inhibition of the PI3K/Akt pathway against breast cancer in a mouse model. *Food Funct*. 2018;9(11):5513–5527. doi:10.1039/c8fo01122b
12. Ahn S, Siddiqi MH, Aceituno VC, et al. Ginsenoside Rg5: rk1attenuates TNF-α/IFN-γ-induced production of thymus- and activation-regulated chemokine (TARC/CCL17) and LPS-induced NO production via down-regulation of NF-κB/p38 MAPK/STAT1 signaling in human keratinocytes and macrophages. *In Vitro Cell Dev Biol Anim*. 2016;52(3):287–295. doi:10.1007/s11626-015-9983-y
13. Hong C, Yang P, Li S, Guo Y, Wang D, Wang J. In Vitro/In vivo metabolism of ginsenoside Rg5 in rat using ultra-performance liquid chromatography/quadrupole-time-of-flight mass spectrometry. *Molecules*. 2018;23(9):2113. doi:10.3390/molecules23092113
14. Sahu SK, Mallick SK, Santra S, Maiti TK, Ghosh SK, Pramanik P. In vitro evaluation of folic acid modified carboxymethyl chitosan nanoparticles loaded with doxorubicin for targeted delivery. *J Mater Sci Mater Med*. 2010;21(5):1587–1597. doi:10.1007/s10856-010-3998-4
15. Koo H, Min KH, Lee SC, et al. Enhanced drug-loading and therapeutic efficacy of hydrotropic oligomer-conjugated glycol chitosan nanoparticles for tumor-targeted paclitaxel delivery. *J Control Release*. 2013;172(3):823–831. doi:10.1016/j.jconrel.2013.08.297
16. Danhier F, Feron O, Préat V. To exploit the tumor microenvironment: passive and active tumor targeting of nanocarriers for anti-cancer drug delivery. *J Control Release*. 2010;148(2):135–146. doi:10.1016/j.jconrel.2010.08.027
17. Nosrati H, Sefidi N, Sharafi A, Danafar H, Manjili HK. Bovine Serum Albumin (BSA) coated iron oxide magnetic nanoparticles as biocompatible carriers for curcumin-anticancer drug. *Bioorg Chem*. 2018;76:501–509. doi:10.1016/j.bioorg.2017.12.033
18. Elzoghby AO, Samy WM, Elgindy NA. Albumin-based nanoparticles as potential controlled release drug delivery systems. *J Control Release*. 2012;157(2):168–182. doi:10.1016/j.jconrel.2011.07.031
19. Kim B, Lee C, Lee ES, Shin BS, Youn YS. Paclitaxel and curcumin co-bound albumin nanoparticles having antitumor potential to pancreatic cancer. *Asian J Pharm Sci*. 2016;11(6):708–714. doi:10.1016/j.ajps.2016.05.005
20. Fang J, Nakamura H, Maeda H. The EPR effect: unique features of tumor blood vessels for drug delivery, factors involved, and limitations and augmentation of the effect. *Adv Drug Deliv Rev*. 2011;63(3):136–151. doi:10.1016/j.addr.2010.04.009
21. Beik J, Khademi S, Attaran N, et al. A nanotechnology-based strategy to increase the efficiency of cancer diagnosis and therapy: folate-conjugated gold nanoparticles. *Curr Med Chem*. 2017;24(39):4399–4416. doi:10.2174/0929867324666170810154917

22. Yang R, An Y, Miao F, Li M, Liu P, Tang Q. Preparation of folic acid-conjugated, doxorubicin-loaded, magnetic bovine serum albumin nanospheres and their antitumor effects in vitro and in vivo. *Int J Nanomedicine*. 2014;9:4231–4243. doi:10.2147/IJN.S67210
23. Shi Y, Su C, Cui W, et al. Gefitinib loaded folate decorated bovine serum albumin conjugated carboxymethyl-beta-cyclodextrin nanoparticles enhance drug delivery and attenuate autophagy in folate receptor-positive cancer cells. *J Nanobiotechnology*. 2014;12(1):43. doi:10.1186/s12951-014-0043-7
24. Lee RJ, Low PS. Delivery of liposomes into cultured KB cells via folate receptor-mediated endocytosis. *J Biol Chem*. 1994;269 (5):3198–3204.
25. Ma N, Liu J, He W, et al. Folic acid-grafted bovine serum albumin decorated graphene oxide: an efficient drug carrier for targeted cancer therapy. *J Colloid Interface Sci*. 2017;490:598–607. doi:10.1016/j.jcis.2016.11.097
26. Neshastehriz A, Tabei M, Maleki S, Eynali S, Shakeri-Zadeh A. Photothermal therapy using folate conjugated gold nanoparticles enhances the effects of 6MV X-ray on mouth epidermal carcinoma cells. *J Photochem Photobiol B*. 2017;172:52–60. doi:10.1016/j.jphotobiol.2017.05.012
27. Kim SN, Ha YW, Shin H, Son SH, Wu SJ, Kim YS. Simultaneous quantification of 14 ginsenosides in Panax ginseng C.A. Meyer (Korean red ginseng) by HPLC-ELSD and its application to quality control. *J Pharm Biomed Anal*. 2007;45(1):164–170. doi:10.1016/j.jpba.2007.05.001
28. Wang L, Li M, Zhang N. Folate-targeted docetaxel-lipid-based-nanosuspensions for active-targeted cancer therapy. *Int J Nanomedicine*. 2012;7:3281–3294. doi:10.2147/IJN.S32520
29. Gharebaghi F, Dalali N, Ahmadi E, Danafar H. Preparation of wormlike polymeric nanoparticles coated with silica for delivery of methotrexate and evaluation of anticancer activity against MCF7 cells. *J Biomater Appl*. 2017;31(9):1305–1316. doi:10.1177/0885328217698063
30. Zhang J, Wang Y, Jiang Y, et al. Enhanced cytotoxic and apoptotic potential in hepatic carcinoma cells of chitosan nanoparticles loaded with ginsenoside compound K. *Carbohydr Polym*. 2018;198:537–545. doi:10.1016/j.carbpol.2018.06.121
31. Mirrahimi M, Hosseini V, Kamrava SK, et al. Selective heat generation in cancer cells using a combination of 808 nm laser irradiation and the folate-conjugated Fe2O3@Au nanocomplex. *Artif Cells Nanomed Biotechnol*. 2018;46(sup1):241–253. doi:10.1080/21691401.2017.1420072
32. Yang Z, Sun N, Cheng R, et al. pH multistage responsive micellar system with charge-switch and PEG layer detachment for co-delivery of paclitaxel and curcumin to synergistically eliminate breast cancer stem cells. *Biomaterials*. 2017;147:53–67. doi:10.1016/j.biomaterials.2017.09.013
33. Yang Z, Sun N, Cheng R, Zhao C, Liu J, Tian Z. Hybrid nanoparticles coated with hyaluronic acid lipoid for targeted co-delivery of paclitaxel and curcumin to synergistically eliminate breast cancer stem cells. *J Mater Chem B*. 2017;5(33):6762–6775. doi:10.1039/C7TB01510K
34. Li JM, Chen W, Wang H, et al. Preparation of albumin nanospheres loaded with gemcitabine and their cytotoxicity against BXPC-3 cells in vitro. *Acta Pharmacol Sin*. 2009;30:1337. doi:10.1038/aps.2009.125
35. Cheng X, Wang X, Cao Z, Yao W, Wang J, Tang R. Folic acid-modified soy protein nanoparticles for enhanced targeting and inhibitory. *Mat Sci Eng C*. 2017;71:298–307. doi:10.1016/j.msec.2016.10.018
36. Zhao D, Zhao X, Zu Y, et al. Preparation, characterization, and in vitro targeted delivery of folate-decorated paclitaxel-loaded bovine serum albumin nanoparticles. *Int J Nanomedicine*. 2010;5:669–677.
37. Dubey RD, Alam N, Saneja A, et al. Development and evaluation of folate functionalized albumin nanoparticles for targeted delivery of gemcitabine. *Int J Pharm*. 2015;492(1):80–91. doi:10.1016/j.ijpharm.2015.07.012
38. Qi L, Guo Y, Luan J, Zhang D, Zhao Z, Luan Y. Folate-modified bexarotene-loaded bovine serum albumin nanoparticles as a promising tumor-targeting delivery system. *J Mater Chem B*. 2014;2 (47):8361–8371. doi:10.1039/C4TB01102C
39. Singh P, Kim YJ, Singh H, Ahn S, Castro-Aceituno V, Yang DC. In situ preparation of water-soluble ginsenoside Rh2-entrapped bovine serum albumin nanoparticles: in vitro cytocompatibility studies. *Int J Nanomedicine*. 2017;12:4073–4084. doi:10.2147/IJN.S125154
40. Mathiyalagan R, Subramaniyam S, Kim YJ, Kim Y-C, Yang DC. Ginsenoside compound K-bearing glycol chitosan conjugates: synthesis, physicochemical characterization, and in vitro biological studies. *Carbohydr Polym*. 2014;112:359–366. doi:10.1016/j.carbpol.2014.05.098
41. Song L, Pan Z, Zhang H, et al. Dually folate/CD44 receptor-targeted self-assembled hyaluronic acid nanoparticles for dual-drug delivery and combination cancer therapy. *J Mater Chem B*. 2017;5(33):6835–6846. doi:10.1039/C7TB01548H
42. Shakeri-Zadeh A, Shiran M-B, Khoee S, Sharifi AM, Ghaznavi H, Khoei S. A new magnetic nanocapsule containing 5-fluorouracil: in vivo drug release, anti-tumor, and pro-apoptotic effects on CT26 cells allograft model. *J Biomater Appl*. 2014;29(4):548–556. doi:10.1177/0885328214536940
43. Nosrati H, Abbasi R, Charmi J, et al. Folic acid conjugated bovine serum albumin: an efficient smart and tumor targeted biomacromolecule for inhibition folate receptor positive cancer cells. *Int J Biol Macromol*. 2018;117:1125–1132. doi:10.1016/j.ijbiomac.2018.06.026
44. Salehiabar M, Nosrati H, Javani E, et al. Production of biological nanoparticles from bovine serum albumin as controlled release carrier for curcumin delivery. *Int J Biol Macromol*. 2018;115:83–89. doi:10.1016/j.ijbiomac.2018.04.043
45. Shen Z, Li Y, Kohama K, Oneill B, Bi J. Improved drug targeting of cancer cells by utilizing actively targetable folic acid-conjugated albumin nanospheres. *Pharmacol Res*. 2011;63(1):51–58. doi:10.1016/j.phrs.2010.10.012
46. Montazerabadi A, Beik J, Irajirad R, et al. Folate-modified and curcumin-loaded dendritic magnetite nanocarriers for the targeted thermo-chemotherapy of cancer cells. *Artif Cells Nanomed Biotechnol*. 2019;47 (1):330–340. doi:10.1080/21691401.2018.1557670
47. Zeinizade E, Tabei M, Shakeri-Zadeh A, et al. Selective apoptosis induction in cancer cells using folate-conjugated gold nanoparticles and controlling the laser irradiation conditions. *Artif Cells Nanomed Biotechnol*. 2018;46(sup1):1026–1038. doi:10.1080/21691401.2018.1443116
48. Ghaznavi H, Hosseini-Nami S, Kamrava SK, et al. Folic acid conjugated PEG coated gold–iron oxide core–shell nanocomplex as a potential agent for targeted photothermal therapy of cancer. *Artif Cells Nanomed Biotechnol*. 2018;46(8):1594–1604. doi:10.1080/21691401.2017.1384384
49. Wu Q, Deng J, Fan D, et al. Ginsenoside Rh4 induces apoptosis and autophagic cell death through activation of the ROS/JNK/p53 pathway in colorectal cancer cells. *Biochem Pharmacol*. 2018;148:64–74. doi:10.1016/j.bcp.2017.12.004